Optimizing the Power Output of a ZnO Photocell by Piezopotential

Youfan Hu,[†] Yan Zhang,[†,‡] Yanling Chang,[†] Robert L. Snyder,[†] and Zhong Lin Wang[†,*]

[†]School of Material Science and Engineering, Georgia Institute of Technology, Atlanta, Georgia 30332-0245 and [‡]Institute of Theoretical Physics, Lanzhou University, Lanzhou Gansu 730000, China

ARTICLE

ABSTRACT Using a metal—semiconductor—metal back-to-back Schottky contacted ZnO microwire device, we have demonstrated the piezoelectric effect on the output of a photocell. An externally applied strain produces a piezopotential in the microwire, which tunes the effective height of the Schottky barrier (SB) at the local contact, consequently changing the transport characteristics of the device. An equivalent circuit model together with the thermionic emission theory has explained the four kinds of relationships observed between the photocurrent and the applied strain. Our study shows the possibility of maximizing the output of a photocell by controlling strain in the device.

KEYWORDS: piezopotential · ZnO · photocell

ZnO is a semiconductor material with a direct band gap and large exciton bonding energy at room temperature and has many exciting applications such as lasers,[1−3] light-emitting diodes,[4−6] and solar cells.[7−9] Most interestingly, the coupled piezoelectric and semiconducting properties of ZnO make it an ideal choice for applications in nanogenerators[10−13] for converting mechanical energy into electricity and in piezotronic devices,[14] such as strain sensors,[15] piezoelectric diodes,[16] and piezoelectric field-effect transistors.[17] Owing to the noncentral symmetric ionic structure of ZnO, polarization of cations and anions occurs in the tetrahedrally coordinated unit of Zn−O under stress. A constructive sum of all of the dipoles in a *c*-axis oriented nanowire results in a macroscopically observable piezoelectric potential (piezopotential), which is created by the nonmobile ions. The principle of the nanogenerator is the piezopotential driven transient flow of electrons in the external load. Piezotronics is about the devices fabricated based on the piezopotential tuned/gated charge carrier transport process.

At a metal−ZnO interface, a Schottky contact can be formed by choosing a proper metal type which can be modified during the engineering process.[18] A Schottky barrier (SB) is favorable to separate the electrons and holes created in the vicinity of the metal−ZnO interface under the excitation of a laser with energy higher than the band gap. If a strain is created in a ZnO nanowire (NW), a piezopotential drop is created along the NW, which may introduce nonsymmetrical changes in the heights of the local Schottky barriers at the two ends of the NW. In this article, the effect of the piezopotential on the output of a photocell is investigated for an M−S−M constructed ZnO microwire photocell. The response of the output current to the applied strain can be divided into four categories. A theoretical calculation showed that they essentially represent different kinds of intrinsic characteristics of the microwire photocell.

RESULTS AND DISCUSSION

Our device was fabricated using a single micro/nanowire of ZnO (see the Experimental Methods for details). The experiment setup is shown schematically in Figure 1. First, all of the devices were tested for the piezoelectric response. Because the microwire was laid on the surface of the substrate and fixed by the two ends, by considering the relative size of the microwire and the substrate, the mechanical behavior of the entire system was dominated by the substrate, and a bending of the flexible substrate produced purely a tensile or compressive strain in the microwire depending on its bending direction. The strain in the microwire can be quantified by the distance at which the substrate was deflected.[15] A typical group of *I*−*V* curves representing the piezoelectric response is shown in Figure 2a. When a ZnO microwire was compressed or stretched along the *c*-axis, a

*Address correspondence to zlwang@gatech.edu.

Received for review May 7, 2010 and accepted May 24, 2010.

Published online Xxxxxxxxx 00, 0000
10.1021/nn1010045

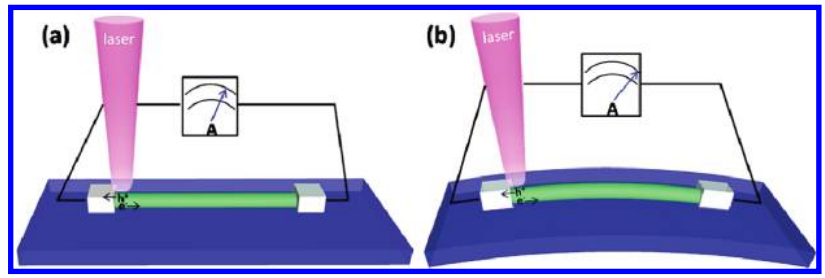

Figure 1. Schematic of the experiment design. (a) Device without strain. (b) Device under strain.

piezopotential drop was created along the microwire. In order to give an intuitive and qualitative description of the effect of the piezopotential, the inset in Figure 2a shows a numerically calculated piezopotential distribution in the wire using the finite element method without considering the natural doping introduced during the synthesis. In this calculation, the dimensions of the wire were assumed to be 900 nm in length and 200 nm in diameter. A force of 80 nN was applied along the axial direction at one end surface of the wire to introduce a compressive or tensile strain, while the other end of the wire was fixed. We can see that the piezopotential changed its sign from one end to the other end of the wire under an axial deformation. When the deformation is switched from compressive into stretching, the polarity of the piezopotential is also switched. This piezoelectric field distribution around the metal−semiconductor contact area in the device will change the effective height of the SB in a different manner at each end and consequently the transport properties of the device, as shown in Figure 2a. It must be mentioned that the applied strain will also change the band structure slightly, which is the piezoresistance effect. This effect also introduces a change in the SB height, but it should be identical at the two ends of the device. While the piezopotential has polarity, it is a nonsymmetric effect at the two ends and is likely to introduce a nonsymmetric variation in the *I*−*V* characteristic.

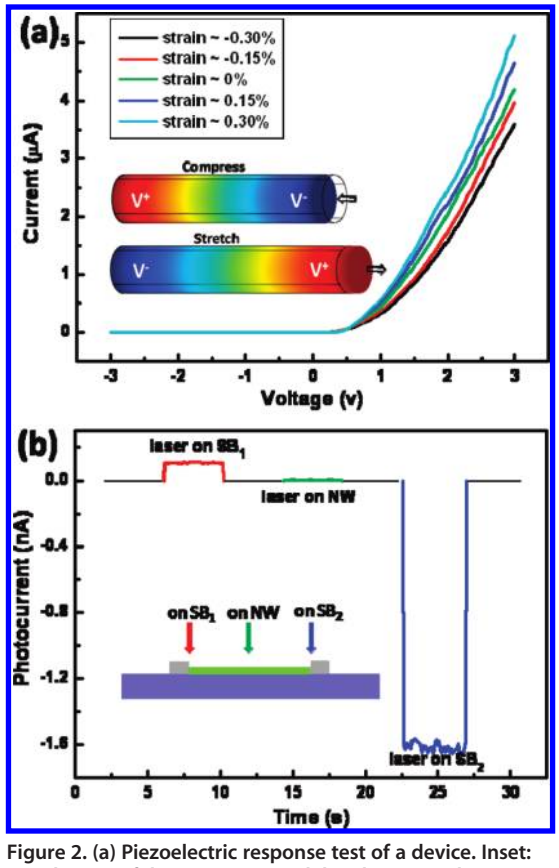

Figure 2. (a) Piezoelectric response test of a device. Inset: Simulations of the piezopotential distribution in the wire under different straining conditions. (b) Measured output current when the laser spot was focused at different positions. The inset shows the sketched picture to indicate the related illuminating position of the laser on the device.

We now use the M−S−M contacted microwire to illustrate the effect of the piezopotential on the performance of a photocell. First, by shining a laser of wavelength 325 nm, the output current was recorded from the device when the laser spot was focused at different positions on the device, as shown in Figure 2b. The entire device is constructed with two back-to-back SBs connected *via* the microwire. When the focal point of the laser beam changed from one SB to the other, the measured output current changed its sign. This is due to the opposite directions of the local electrical fields at the two SB areas, which enforce the separation of electrons and holes induced by the laser irradiation and thus lead them to flow in opposite directions. If we fixed the laser beam at one SB area and bend the substrate of the device step-by-step, strain will be introduced into the device step-by-step. Depending on the deformation direction, the sign of the strain is changed from negative to positive or *vice versa*. Meanwhile, the corresponding piezopotential distribution in the wire will also be adjusted step-by-step. This will alter the effective heights of the two SBs and thus the characteristic of the microwire photocell.

Four kinds of characteristic relationships between the output current and the applied strain have been observed. The first one is that the output current increases with applied strain, as shown in Figure 3a. We have tested 26 devices, and 14 of them exhibited this type of behavior. The second kind is just opposite to the first one: the output current decreases when the applied strain is increased (Figure 3b). Only 2 devices out of the 26 had this type of output current characteristic. The third kind and the fourth are similar. They both have a

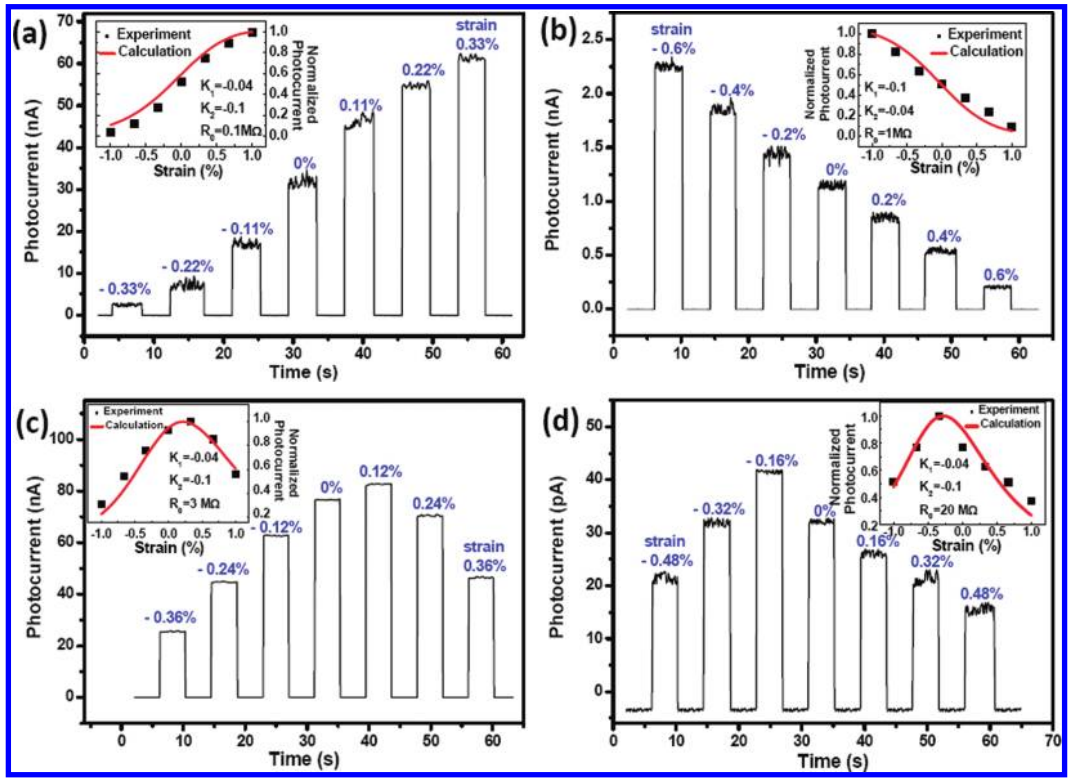

Figure 3. Output current responses to the strain applied on the device, which can be divided into four categories: (a) increasing, (b) decreasing, and with a maximum under (c) applying positive strain or (d) negative strain. The inset is the calculated results to indicate the output current behavior based on the related parameters, showing a similar changing trend compared with the experimental data after normalization.

maximum output current responding to the applied strain, but for the former one, the maximum point occurred in the tensile strain range (Figure 3c), while the latter is in the compressive strain range (Figure 3d). Among the 26 devices, 6 devices were in the third case and 4 in the fourth one. These different behaviors indicated some intrinsic difference in these photocells.

The coupling among the optical, mechanical, and electrical properties in these ZnO devices provides a new method to distinguish and probe their intrinsic characteristics. Their behavior can be quantitatively understood based on an equivalent circuit simulation together with thermionic emission theory for the photocell. When a laser beam with a fixed power is focused at the SB area, this part worked as a constant photocurrent source, which is connected in parallel with a forward biased Schottky diode (referred to as SD_1) that characterizes the role played by the SB. The output current we measured is the current that passes through the rest of the circuit, which is the other forward biased Schottky diode at the opposite end of the device (referred to as SD_2) and the microwire. When a strain is introduced into the device *via* bending, the SB height and the resistance of the microwire are all changed correspondingly. These three parts will serve as three rheostats (R_1, R_2, and R_0) that are a function of the strain. The coupling among these variable electronic parameters and their matching with the load produces various output configurations, as elaborated in what follows.

On the basis of the characteristics of the equivalent circuit (Figure 4b), we have

$$I = I_1 + I_2 \quad (1)$$

$$V = I_2 R_0 + V_2 \quad (2)$$

in which I is the constant photocurrent induced by the laser irradiation, I_1 and I_2 are the currents passing through the corresponding circuit branch where SD_1 and SD_2 are contained, and V and V_2 are the voltage drops on the constant photocurrent source and SD_2. For a forward biased Schottky diode, the current passing through can be described by thermionic emission theory:[19]

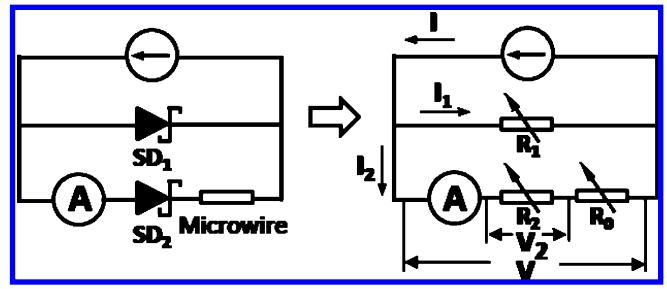

Figure 4. Structure of a microwire photocell circuit and its corresponding equivalent circuit for theoretical calculation.

$$I_1 = I_{1s}\left[\exp\left(\frac{qV}{kT}\right) - 1\right] \quad (3)$$

$$I_2 = I_{2s}\left[\exp\left(\frac{qV_2}{kT}\right) - 1\right] \quad (4)$$

where

$$I_{1s} = S_1 A^* T^2 \exp\left(-\frac{q\phi_2}{kT}\right) \quad (5)$$

$$I_{2s} = S_2 A^* T^2 \exp\left(-\frac{q\phi_2}{kT}\right) \quad (6)$$

in which S_1 and S_2 are the Schottky contact areas and ϕ_1 and ϕ_2 are the SB heights for SD_1 and SD_2, respectively, A^* is the Richardson constant for thermionic emission, T is the temperature, q is the electron charge, and k is the Boltzmann constant.

If, $qV/kT \ll 1$, we can get the analytical solution of the measured output current I_2 from eqs 1−4 as

$$I_2 = \frac{\alpha I}{\alpha\left(\frac{I_{1s}}{I_{2s}} + 1\right) + R_0 I_{2s}} \quad (7)$$

where $\alpha = kT/q$. If this condition cannot be met, we also checked the numerical solutions for I_2. We found that, for the same parameters, the analytical and numerical solutions showed the same variation trend, and there were only some small differences in the current magnitude for the final simulation data. So, in order to get a more intuitive analysis, we assume that eq 7 always holds.

We can define a function $f(\varepsilon)$ as

$$f(\varepsilon) = \alpha\left(\frac{I_{2s}}{I_{2s}} + 1\right) + R_0 I_{2s} \quad (8)$$

in which ε is the applied strain. According to the experimental results, the variation of R_0 in responding to strain can be ignored. Our previous experimental results[15] showed that, for a small strain range, we can introduce an empirical expression:

$$\begin{cases}\phi_1 = K_1\varepsilon + \phi_{10} \\ \phi_2 = K_2\varepsilon + \phi_{20}\end{cases} \text{and} \begin{cases}K_1 < 0 \\ K_1 < 0\end{cases} \quad (9)$$

Thus, On the basis of eqs 5, 6, and 8, we can get

$$\frac{df(s)}{ds} = \left(-\frac{1}{kT}\right) I_{1s} K_1 [R' + R_0] \quad (10)$$

in which

$$R' = \frac{\alpha}{I_{2s}}\left(1 - \frac{K_2}{K_1}\right) \quad (11)$$

Case 1: If $|K_1| > |K_2|$, $df(\varepsilon)/d\varepsilon > 0$, I_2 will be a decreasing function of ε, corresponding to the case observed in Figure 3b.

Case 2: If, $|K_1| < |K_2|$, the sign of $df(\varepsilon)/d\varepsilon$ depends on the relative magnitude between $|R'|$ and R_0.

Because I_{2s} is a function of ϕ_2, R' will change its magnitude when strain is applied. Thus, under a proper straining condition, we have the following subcases:

Case 2-a: when $|R'| > R_0$, $df(\varepsilon)/d\varepsilon < 0$, I_2 is a increasing function of ε.

Case 2-b: when $|R'| = R_0$, $df(\varepsilon)/d\varepsilon = 0$, I_2 will reach its maximum at this point.

Case 2-c: when $|R'| < R_0$, $df(\varepsilon)/d\varepsilon > 0$, I_2 is a decreasing function of ε,

Because the strain we applied was a limiting extent, the variation range of $|R'|$ is restricted. If $|R'| \gg R_0$ is the initial state of the device, the change of $|R'|$ will be for the strain range of Case 2-a, which corresponds to the result presented in Figure 3a. Similarly, if the initial states of the device is $|R'| \ll R_0$, the change of $|R'|$ will be for Case 2-c, and the corresponding result is shown in Figure 3b. Finally, if $|R'|$ R is comparable with the value of R_0, I_2 reaches its maximum in the positive (Figure 3c) or negative (Figure 3d) strain range depending on the initial relative magnitude of the two values.

From the statistical point of view, the probability for having $|K_1| > |K_2|$ and $|K_1| < |K_2|$ should be equal. Thus, the monotonic decreasing case should be observed more than half the time in fabricated devices. This is not the case observed in our experiments. As we have shown previously, the free electrons in the n-type ZnO will partially screen the piezoelectric field.[20] Since the laser beam was focused on the SD_1 area, the free carrier density at this local region was increased drastically under laser irradiation. In such a case, the effect introduced by the piezopotential was much reduced at this local region.[21] Therefore, in most cases, $|K_1| < |K_2|$. In reference to the distribution of device characteristics as elaborated in Figure 3, most of the devices met the criterion of $|R'| > R_0$ (Case 2-a). Therefore, the four different photocurrent behaviors presented in Figure 3 represent the different intrinsic characteristics of microwire photocells.

In order to examine the intrinsic role played by $|K_1/K_2|$ and $|R'/R_0|$ as stated above, we calculated the output current from eq 7 as a function of these two parameters. The related experimental data were plotted comparing these calculated results after normalization. We fixed $\phi_{10} = \phi_{20} = 0.4$ eV, and $I = 10^{-\varepsilon}$ A for all of the cases. We chose $K_1 = -0.04$, $K_2 = -0.1$, which is the typical value obtained from the experiments; when R_0 is changed from 0.1 to 3 MΩ and then to 20 MΩ, the photocurrent behaviors changed from increasing trend, with a maximum point at the positive strain range and then to a maximum point at the negative strain range, as shown in the insets of Figure 3a,c,d, respectively. When we chose $K_1 = -0.1$, $K_2 = -0.04$, and $R = 1$ MΩ, a decreasing behavior of the photocurrent was obtained, as shown in the inset of Figure 3b. These simulated results agree with the experimental data quantitatively in the overall trend.

CONCLUSION

In summary, using a metal−semiconductor−metal back-to-back Schottky contacted ZnO microwire device, we have demonstrated the piezoelectric effect on the output of the photocell. An externally applied strain produces a piezopotential in the microwire, which tunes the effective Schottky barrier height of the microwire at the local contact, consequently changing the electrical parameter of the device. By properly tuning the strain in a device, it is possible to maximize the output power of a photocell, light-emitting diode, and solar cells. A study of the coupling among the optical, mechanical, and electrical properties of ZnO provides new approaches for fabricating piezophototronic devices.[22]

EXPERIMENTAL METHODS

The ultralong ZnO microwires used in our study were grown by a high-temperature thermal evaporation process.[22] For fabricating a ZnO microwire photocell, a ZnO microwire was first laid down on a polystyrene (PS) substrate, and then each end of the wire was fixed to the substrate using silver paste. The dimension of the PS substrate was 3.5 mm long, 5 mm wide, and 1 mm thick. An additional very thin layer of polydimethylsiloxane (PDMS) was used to package the device, and it kept the device mechanically robust under repeated manipulation. Flexible and transparent microwire photocells were obtained after drying in air for 48 h. The experimental design is sketched in Figure 1. The strain was introduced *via* bending the substrate by a precisely controlled linear stage (MFA-CC, Newport Corp.) with a motion resolution of 0.0175 μm. A He−Cd laser beam (wavelength = 325 nm, diameter < 20 μm) was focused at the designed position on the device. We utilized a UV enhanced CCD camera to act as the monitor. A Keithley 4200 semiconductor characterization system was used to carry out electrical measurement.

Acknowledgment. Research was supported by NSF (DMS 0706436, CMMI 0403671, ENG/CMMI 112024), DARPA (Army/AMCOM/REDSTONE AR, W31P4Q-08-1-0009), BES DOE (DE-FG02-07ER46394), DARPA/ARO W911NF-08-1-0249, World Premier International Research Center (WPI) Initiative on Materials Nanoarchitectonics, MEXT, Japan.

REFERENCES AND NOTES

1. Nicoll, F. H. Ultraviolet ZnO Laser Pumped by an Electron Beam. *Appl. Phys. Lett.* **1966**, *9*, 13–15.
2. Bagnall, D. M.; Chen, Y. F.; Zhu, Z.; Yao, T.; Koyama, S.; Shen, M. Y.; Goto, T. Optically Pumped Lasing of ZnO at Room Temperature. *Appl. Phys. Lett.* **1997**, *70*, 2230–2232.
3. Zimmler, M. A.; Bao, J.; Capasso, F.; Muller, S.; Ronning, C. Laser Action in Nanowires: Observation of the Transition from Amplified Spontaneous Emission to Laser Oscillation. *Appl. Phys. Lett.* **2008**, *93*, 051101.
4. Tsukazaki, A.; Ohtomo, A.; Onuma, T.; Ohtani, M.; Makino, T.; Sumiya, M.; Ohtani, K.; Chichibu, S. F.; Fuke, S.; Segawa, Y.; Ohno, H.; Koinuma, H.; Kawasaki, M. Repeated Temperature Modulation Epitaxy for p-Type Doping and Light-Emitting Diode Based on ZnO. *Nat. Mater.* **2005**, *4*, 42–46.
5. Ryu, Y.; Lee, T.-S.; Lubguban, J. A.; White, H. W.; Kim, B.- J.; Park, Y.-S. Next Generation of Oxide Photonic Devices: ZnO-Based Ultraviolet Light Emitting Diodes. *Appl. Phys. Lett.* **2006**, *88*, 241108.
6. Bao, J.; Zimmler, M. A.; Capasso, F. Broadband ZnO Single-Nanowire Light-Emitting Diode. *Nano Lett.* **2006**, *6*, 1719–1722.
7. Baxter, J. B.; Aydil, E. S. Nanowire-Based Dye-Sensitized Solar Cells. *Appl. Phys. Lett.* **2005**, *86*, 053114.
8. Law, M.; Greene, L.; Johnson, J. C.; Saykally, R.; Yang, P. Nanowire Dye-Sensitized Solar Cells. *Nat. Mater.* **2005**, *4*, 455–459.
9. Weintraub, B.; Wei, Y.; Wang, Z. L. Optical Fiber/Nanowire Hybrid Structures for Efficient Three-Dimensional Dye-Sensitized Solar Cells. *Angew. Chem., Int. Ed.* **2009**, *48*, 1–6.
10. Wang, Z. L.; Song, J. H. Piezoelectric Nanogenerators Based on Zinc Oxide Nanowire Arrays. *Science* **2006**, *312*, 242–246.
11. Wang, X. D.; Song, J. H.; Liu, J.; Wang, Z. L. Direct-Current Nanogenerator Driven by Ultrasonic Waves. *Science* **2007**, *316*, 102–105.
12. Qin, Y.; Wang, X. D.; Wang, Z. L. Microfibre Nanowire Hybrid Structure for Energy Scavenging. *Nature* **2008**, *451*, 809–813.
13. Chang, C.; Tran, V. H.; Wang, J. B.; Fuh, Y.-K.; Lin, L. W. Direct-Write Piezoelectric Polymeric Nanogenerator with High Energy Conversion Efficiency. *Nano Lett.* **2010**, *10*, 726–731.
14. Wang, Z. L. The New Field of Nanopiezotronics. *Mater. Today* **2007**, *10*, 20–28.
15. Zhou, J.; Gu, Y. D.; Fei, P.; Mai, W. J.; Gao, Y. F.; Yang, R. S.; Bao, G.; Wang, Z. L. Flexible Piezotronic Strain Sensor. *Nano Lett.* **2008**, *8*, 3035–3040.
16. He, J. H.; Hsin, C. L.; Liu, J.; Chen, L. J.; Wang, Z. L. Piezoelectric Gated Diode of a Single ZnO Nanowire. *Adv. Mater.* **2007**, *19*, 781–784.
17. Wang, X. D.; Zhou, J.; Song, J. H.; Liu, J.; Xu, N. S.; Wang, Z. L. Piezoelectric Field Effect Transistor and Nanoforce Sensor Based on a Single ZnO Nanowire. *Nano Lett.* **2006**, *6*, 2768–2772.
18. Gao, Z. Y.; Zhou, J.; Gu, Y. D.; Fei, P.; Hao, Y.; Bao, G.; Wang, Z. L. Effects of Piezoelectric Potential on the Transport Characteristics of MetalZnO NanowireMetal Field Effect Transistor. *J. Appl. Phys. Lett.* **2009**, *105*, 113707.
19. Sze, S. M. *Physics of Semiconductor Devices*, 2nd ed.; Wiley: New York, 1981.
20. Gao, Y. F.; Wang, Z. L. Equilibrium Potential of Free Charge Carriers in a Bent Piezoelectric Semiconductive Nanowire. *Nano Lett.* **2009**, *9*, 1103–1110.
21. Hu, Y. F.; Chang, Y. L.; Fei, P.; Snyder, R. L.; Wang, Z. L. Designing the Electric Transport Characteristics of ZnO Micro/Nanowire Devices by Coupling Piezoelectric and Photoexcitation Effects. *ACS Nano* **2010**, *4*, 1234–1240.
22. Pan, Z. W.; Dai, Z. R.; Wang, Z. L. Nanobelts of Semiconducting Oxides. *Science* **2001**, *291*, 1947–1949.